East European Journal of Physics. 3. 478-490 (2026)
DOI: 10.26565/2312-4334-2026-3-43 ISSN 2312-4334

AB-INITIO INVESTIGATION OF THE PHYSICAL FEATURES OF Pt-Co INTERMETALLIC COMPOUNDS

H. Grimed[1,2], R. Boulechfar[1], H. Ben Sadallah[1], F. Semari[4], Y. Khenioui[5], D. Sayad[3], M. Boudjelal[4], H. Meradji[6]*, S. Ghemid[6], D. Singh[7], R. Khenata[4,8]

[1]*Laboratoire des matériaux et génie énergétique (LMGE), Université 20 Août 1955-Skikda, Algeria*
[2]*Laboratoire LRPCSI, Université du 20 Août1955, B.P 26, Skikda, 21000, Algeria*
[3]*Laboratoire d'Electronique de Skikda (LRES), Department of Electrical Engineering, University 20 Aout 1955-Skikda, 21000, Skikda, Algeria*
[4]*Laboratoire de Physique Quantique de la Matière et de Modélisation Mathématique, Université de Mascara, 29000, Mascara, Algeria*
[5]*Department of Structure and Cladding Materials, Division of Fuel Technology, Draria Nuclear Research Center, PB 43, Sebala, Draria, Algiers, Algeria*
[6]*Radiation Physics Laboratory, Department of Physics, Faculty of Sciences, Badji Mokhtar University, Annaba, Algeria*
[7]*Department of Physics, Prof. Rajendra Singh (Rajju Bhaiya) Institute of Physical Sciences for Study and Research, Veer Bahadur Singh Purvanchal University, Jaunpur-222003, U.P., India*
[8]*Algerian Academy of Sciences and Technologies, Rais Hamidou Villa- El Madania, Algiers 16000, Algeria*
**Corresponding Author Email: hocine.meradji@univ-annaba.dz*
Received April 2, 2026; revised July 11, 2026; accepted August 21, 2026

This article explores the structural, electronic, mechanical, magnetic, and thermodynamic properties of Pt-Co intermetallic compounds using the FP-LAPW (full-potential linearized augmented plane wave) method within the DFT (density functional theory) framework, as implemented in the Wien2k code. The negative formation enthalpies and cohesive energies indicate that Pt_3Co ($L1_2$), PtCo ($L1_0$), and $PtCo_3$ ($L1_2$) are stable in the ferromagnetic (FM) phase. The calculations of the lattice constants and bulk modulus align with existing theoretical and experimental values. The resulting electronic band structure establishes the metallic nature and the magnetic character of all three studied compounds. The DOS at the Fermi level, the electronic specific heat coefficient γ_{th}, polarization P%, and magnetic moment are determined. The investigation of the elastic and mechanical features illustrates that the selected materials are stable and slightly anisotropic. The Pt_3Co and $PtCo_3$ materials are inherently ductile and the PtCo is the harder compound. To enhance understanding of these materials, the quasi-harmonic Debye model is applied to scrutinize their thermal features.
Keywords: *DFT; FP-LAPW; Intermetallic; Electronic Properties; Mechanical constants*

1. INTRODUCTION

Pt-based alloys, in particular, are among the most vital intermetallic materials, finding extensive use in medical devices, thermoelectrics, and electrodes [1, 2]. Alloys of transition metals have gained importance as magnetic materials due to their potential for high-density magnetic recording [3-8]. These systems are especially noteworthy due to Pt extensive role in heterogeneous catalysis and electrochemistry [9-14]. These materials are sought after for an extensive variety of applications, together with high-density magnetic data recording [4], magneto-optics [15-19], magnetic random-access memory (MRAM) [16], oxygen reduction catalysis [16, 20-23], data storage [24], and biomedicine [25]. In the bulk Pt-Co binary alloys, three ordered phases Pt_3Co ($L1_2$), PtCo ($L1_0$), and $PtCo_3$ ($L1_2$) appear in the phase diagram [26]. These compounds have accomplished exceptional consideration in the contemporary expertise for their numerous physical characteristics. Currently, the ordered $L1_2$-Pt_3Co and $L1_2$-$PtCo_3$ compounds are widely used as in the oxygen reduction reaction (ORR) [27-36]. PtCo catalysts exhibit higher ORR activity which makes them as promising ORR catalysts [37-40].

In the scheme of DFT the Pt-based alloys and Pt-Co alloys are the subject of several studies. Gavira *et al*. [41] calculated the mechanical, magnetic, and electrical features of Pt-Co alloys and the superlattice structures Pt_3Co $L1_2$ and PtCo $L1_0$ using DFT. Karoui *et al*. [42] examined the role of magnetism in the formation energies of Co-Pt alloys using non-spin-polarized and spin-polarized ab initio computations to evaluate the stability of the $L1_0$ and $L1_2$ structures with the ABINIT code [43]. Boulechfar *et al.* inspected the stability and ductility of Pt_3Sc and Pt_3Y materials with directed covalent bonding and confirmed the structural stability [44] using the FP-LAPW technique. This later process is employed to study the magnetic and optical features of Pt_3V and Pd_3V compounds. Along with the fundamental properties such as structural, electronic and mechanical properties, the nonmagnetic and ferromagnetic states calculations indicate that the FM-$D0_{22}$ is the most stable, and pseudo gap is owing to the strong *d-d* hybridization in both ductile compounds [45]. Front *et al.* [46] measured mixing enthalpies for concentrated alloys or dissolution enthalpies in the diluted limits of Pt(Co) and Co(Pt), and lattice parameters evaluated by DFT-GGA/PW91 [47], TB-SMA potential. Alsaad *et al.* [24] explored the structural, electronic, and magnetic characteristics of M_XPt_{x-1} (M: V, Ni and Co) by means of the VASP. Chepulskii *et al*. [48] concentrated on adjusting the $L1_0$ atomic order in Co-Pt nanoparticles, providing ab initio perceptions through Monte Carlo simulations. They demonstrated

Cite as: H. Grimed, R. Boulechfar, H. Ben Sadallah, F. Semari, Y. Khenioui, D. Sayad, M. Boudjelal, H. Meradji, S. Ghemid, D. Singh, R. Khenata, East Eur. J. Phys. 3, 478 (2026), https://doi.org/10.26565/2312-4334-2026-3-43

that $L1_0$ is an adaptable structure within the fcc-constrained ground-state phase illustration of Co-Pt. Li *et al.* [49] performed the influences of pressure on the structural, electronic, mechanical, and thermodynamic features of the typical Pt_3M (M: Al, Sc, Co, Y, Hf, Zr) materials using the VASP [50]. The authors observed that the charge distribution remains largely unchanged, suggesting that no phase transition takes place within the 0–100 GPa range. Furthermore, Zosiak *et al*. [51] studied the electronic structure of Co-Pt-grounded arrangements, from bulk to nano alloys, using ab initio methods. Zhang *et al.* employed the (VASP) code to address the plastic behavior of Pt_3Hf compound [52]. Aledealat *et al.* employed Monte Carlo simulation and DFT to examine the magnetic and electronic features of binary alloys X_3Pt and XPt_3 (X: Ni, Co, or Fe), in $L1_2$ structure and the ferromagnetic states [53]. They calculated Curie temperature (*Tc*) and the magneto crystalline anisotropy for the studied alloys. By means of the CASTEP, the fundamental physical features are investigated for Pt_3X (X = Ti, Cu) [54] and Pt_3T (T: Ni, Mn) [55] intermetallic compounds. More recently, Wei [56] examined the effect of atomic doping (Au, Ir, Os, Pd, Rh, Ru) on the ground states features of Pt-based alloys using first-principles methods. The study revealed that doping increases the dislocation energy and reduces the plasticity of the solid solution.

In recent years, the $L1_0$-ordered intermetallic compounds FeX and CoX (X is a *d* transition metal) were studied using both first-principles calculations and experimental methods. Rani *et al.* explored the magnetism of $L1_0$-FeNi alloy through inducing tetragonal distortion with the interstitial doping. The results show that the structural distortion induces enormous magneto crystalline anisotropy (MCA) and the rise in MCA is larger for N-doping in Ni-layer than in Fe-layer [57]. Aledealat *et al.* [16] in the theoretical study of the magnetic features of $L1_0$-ordered FeM (M: Ni, Pt or Pd) alloys, report that the ferromagnetic configuration is the furthermost stable spin arrangement for the compounds in interest, and FePt alloy possesses a large magnetocrystalline anisotropy. Islam *et al.* [58] investigated ordered $L1_0$-CoPt nanoparticles using both experimental techniques and DFT calculations. Lethole *et al.* [5] studied mechanical, electronic, magnetic, and dynamical characteristics of M-Pt alloys (M: Mn, Ni and Co). Their achieved values reveal that MnPt and NiPt alloys stay stable at 0 K, whereas, CoPt remains marginally metastable aligning fairly well with most experimental phase stability diagrams. Recently, Zine *et al.* conducted a theoretical investigation on the structural, magnetic, electronic, and thermodynamic properties of Tetrataenite $L1_0$-FeNi alloy [59]. Subsequently, they investigated the impacts of cobalt (Co) doping on the $L1_0$-FeNi alloy [60]. The results show that the FeNi:Co(O_{Ni}) in $L1_0$-structure exhibits a big enrichment in saturation magnetization (M_s) and magnetic moments. Co-substituted FeNi alloys grasp potentials as budding entrants for the rare-earth-free permanent magnets. Notice that, according to the previous works three Pt-Co compounds possess ferromagnetic state, Pt_3Co [61, 62], PtCo [63-65] and $PtCo_3$ [63,64]. These alloys are of particular interest due to their remarkable structural and magnetic properties, as well as their wide range of applications in emerging technologies.

Although numerous studies have explored these alloys, there is still a deficiency of comprehensive research work on the detailed physical features of Pt_3Co, PtCo and $PtCo_3$ in the existing data. Consequently, the principal objective of the present investigation is to explore the impressive physical features of Pt_3Co, PtCo and $PtCo_3$ compounds, and understand the physical origins of their distinct characteristics. In this study, using the FP-LAPW technique, we explored the structural stability, the electronic, mechanical magnetic and thermodynamic features for compounds in question, in non-magnetic (NM) and ferromagnetic (FM) states.

2. COMPUTATIONAL DETAILS

The computations reported in the current investigation have been accomplished with the help of the Wien2K code [66] based on full-potential linear augmented plane-wave (FP-LAPW) technique [67] inside the framework of DFT. The generalized gradient approximation (GGA) plus Perdew–Burke–Ernzerhof (PBE) parameterization was utilized for the exchange–correlation functional [50, 68]. The cut-off parameter has been set to $R_{MT}\times K_{max} = 9$, where R_{MT} is the muffin-tin sphere radius and K_{max} is the highest value of the plane wave vector. To calculate the entire energy, 84 special k-points are exploited for the irreducible Brillouin zone in the $L1_2$ structure and 75 for the $L1_0$structure, l_{max} =10 and the charge density is Fourier-expand fit for G_{max}=13. For the muffin-tin sphere radii, we applied R_{MT} (Pt)=2.25 a.u, R_{MT} (Co)=2.00 a.u. The changes in total energy during the optimization ultimately converge to 10^{-4} Ry. The valence electron configurations: Pt: [Xe]. $4f^{14}\ 5d^9\ 6S^1\ 6p^0$ and Co: [Ar]. $4S^2\ 4p^0\ 3d^7\ 4f^0$.

3. RESULTS AND DISCUSSION

3.1. Structural features

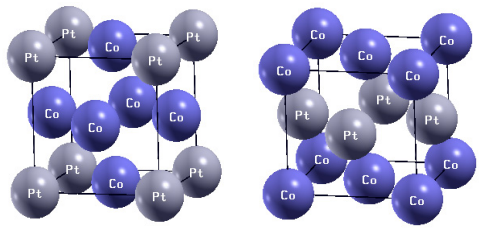

a b

Figure 1. $PtCo_3$ in $L1_2$ structure (a) and PtCo in $L1_0$ structure (b)

The Pt-Co alloy is recognized to have a robust propensity for assembling so as to its phase diagram has been investigated by three key ordered phases, the Pt_3Co ($L1_2$), PtCo ($L1_0$) and $PtCo_3$ ($L1_2$). Both compounds with stoichiometry A_3B crystallize in the cubic $L1_2$ structure (*Prototype: Cu_3Au*) with space group $Pm\bar{3}m$ (*cP4*), where the B atoms occupy the corners of the cube 1*a* (0, 0, 0), and the A atoms set on the face centres 3*c* (1/2, 1/2, 0). PtCo compound crystallizes in tetragonal $L1_0$ (*Prototype*: *AuCu*) with space group *P4/mmm* (*tP2*). This is a tetragonal distortion of the fcc structure and has two of the faces occupied by one type of atom (1*c* (1/2, 1/2, 0)) and the corner (1*a* (0, 0,0)), and the other face occupied with the second type of atom (*2e* (0, 1/2, 1/2)) (Fig. 1**)**.

To determine the structural features, the overall energy is evaluated in relation to the global volume for Pt_3Co, PtCo, and $PtCo_3$ compounds for both nonmagnetic and ferromagnetic states in the $L1_2$ and $L1_0$ structures. The overall energy values in relation to unit cell volume have been tailored via Murnaghan's equation of state [69]. The attained data by means of PBE-GGA approximation have been exposed in Fig. 2.

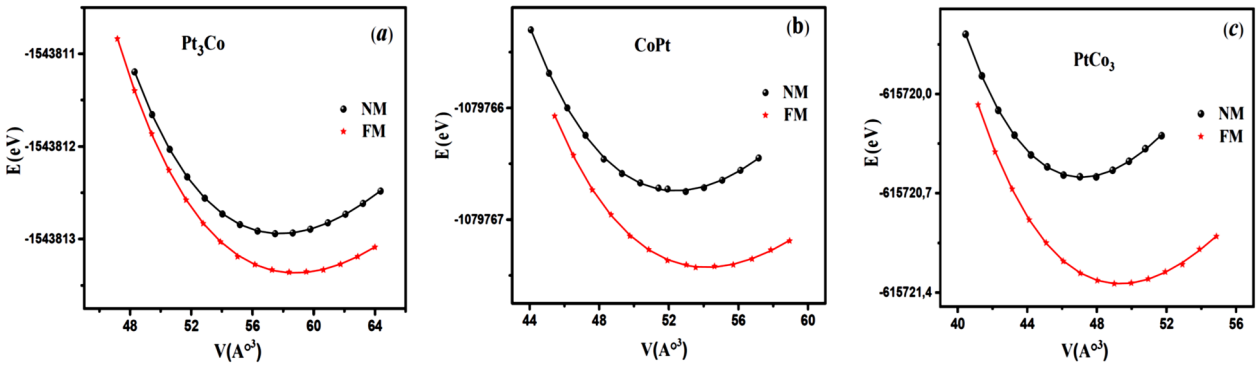

Figure 2. Entire energy vs. volume in the nonmagnetic (NM) and ferromagnetic (FM) states of (a) Pt_3Co, (b) PtCo and (c) $PtCo_3$

It can be perceived that the total energy of the ferromagnetic state is far less than that of nonmagnetic states, demonstrating that the FM state is the magnetic ground state for all materials deliberated here. The overall energy difference (ΔE) between FM and NM states at equilibrium is calculated as follows:

$$\Delta E = E_{FM} - E_{NM} \quad (1)$$

The equilibrium total energy calculation determines the crucial physical parameters such as the cohesive energy E_c and formation enthalpy ΔH_f and describes the structural stability. The values of E_c have been evaluated using the succeeding formula:

$$E_c = \left(\frac{1}{x+y}\right)\left[E_{tot}^{Pt_xCo_y} - xE_{tot}^{atom(Pt)} - yE_{tot}^{atom(Co)}\right] \quad (2)$$

where $E_{tot}^{Pt_xCo_y}$ is the aggregate energy of Pt_xCo_y alloy and $E_{tot}^{atom(Pt)}$ and $E_{tot}^{atom(Co)}$ are the energies of the isolated atoms Pt and Co, respectively.

The enthalpy of formation of these alloys was determined using:

$$\Delta H_f = \left(\frac{1}{x+y}\right)\left[E_{tot}^{Pt_xCo_y} - xE_{tot}^{Pt(solid)} - yE_{tot}^{Co(solid)}\right] \quad (3)$$

where $E_{tot}^{Pt(solid)}$ and $E_{tot}^{Co(solid)}$ are the energies per atom of Pt and Co in the solid-state, correspondingly.

In Table 1, the obtained values of ΔE, E_c and ΔH_f are equated with accessible experimental and theoretical information.

Table 1. ΔE (meV/atom), ΔH_f (eV/atom), referred to Co(fcc)/Co(hcp) and Pt (fcc) and E_c (eV/atom), for Pt_3Co, PtCo and $PtCo_3$ for both nonmagnetic (NM) and ferromagnetic (FM) cases

Compounds	ΔE	ΔH_f (NM)	ΔH_f (FM)	E_c (NM)	E_c (FM)
Pt_3Co	-106*	-0.029*/-0.034*	-0.089*/-0.084* -0.07[a] /- -/-0.1[b] -/-0.12[c] -0.067[d]/- -0.0745[e]/-	-0.802*	-0.055*
PtCo	-172*	-0.022*/-0.028* -0.02 [a] / - -0.0354[e]/ -	-0.099*/-0.088* -0.1[a] / - - /-0.110 [b] -/-0.07[c] -0.099[d]/- -0.095[f]/- -0.079[j]/- -0.089[h]/-	-2.781*	-1.96*
$PtCo_3$	-471*	-0.018*/-0.034*	-0.07*/ -0.057* -0.07[a]/- -/-0.1[b] -0.0688[d]/-	-4.69*	-3.875*

*Our calculation: [a]Ref. [42] PAW, [b]Ref. [51] PP-GGA, [c]Ref. [73] Exp, [d]Ref. [8] PP-PAW, [e]Ref. [74], PP-PAW- GGA, [f]Ref. [65] KKR-CPA, [j]Ref. [65] PP-LDA, [h]Ref. [65] PP-GGA.

The overall energy difference ΔE at the equilibrium volume, in meV/atom unit, is ordered as follows: $PtCo_3$(-471)<PtCo(-172)<Pt_3Co (-106). ΔE have a considerable value for $PtCo_3$ case, with high Co concentration, which specifies the decisive part of the spin effect in the thermodynamic stability.

The enthalpies of formation assist in predicting the stability of alloys and helps in developing their phase diagrams [70]. The formation enthalpy results are evaluated relative to the Co-fcc/Co-hcp and Pt-fcc states. From Table 1, it can be observed that the studied compounds exhibit negative enthalpies of formation for the NM and FM states, suggesting that they are chemically stable and readily synthesized. According to the present findings, 3 materials' alloying abilities are as follows: PtCo>Pt_3Co>$PtCo_3$. For FM states, lower formation enthalpies correspond to larger alloying ability [71,72], whereas, for NM states, the formation enthalpies are ordered as Pt_3Co >PtCo >$PtCo_3$. On the other hand, for each compound the ΔH_f for FM states is lower than the NM states. The negative valued cohesive energies suggest that all compounds are stable in the considered phases. The $PtCo_3$ compound possesses the higher structural stability due to the larger cohesive energy relative to the PtCo and Pt_3Co. It can be concluded that the cubic (tetragonal) $PtCo_3$ (PtCo) and Pt_3Co compounds crystalize in the FM-$L1_2$ (FM-$L1_0$) phase and these results agree well with experimental phase diagram [70]. Comparatively, our results (ΔH_f values) are in upright promise with several reported values [8,42,51,65,73,74] (Table 1). However, as far as we know, there are no accessible information in the literature for cohesive energies.

The equilibrium lattice constants (*a* and *c*), bulk modulus, *B*, and its pressure derivative B′ follow from an appropriate form of the entire energy in terms of volume to the (MEOS) Murnaghan equation of state [69]. The key results are summarized in Table 2. The comparison with the experimental results [75,77-79] and theoretical results [8,24,51,65,76] shows good overall agreement for a, c, and *B*. Both computations effectively forecast the durable impact of magnetism on chemical ordering. The results for a and c are in good agreement with the available experiments. The discrepancy between the evaluated equilibrium volumes and the corresponding experimental values is less than 2.4%.

Table 2. a (in Å), c (in Å), and c/a ratio, B in (GPa), and B′ for Pt_3Co, PtCo, and $PtCo_3$ compounds

Compounds	Method	a	c	c/a	B	B′
Pt_3Co	This work					
	GGA(NM)	3.86*	-	-	225*	5.01*
	GGA(FM)	3.88*	-	-	304*	4.74*
	Experimental	3.831[a]	-	-	-	-
	Other calculations					
		3.871[b]	-	-	-	-
		3.89[c]	-	-	-	-
	NM	3.87[d]	-	-	268.4[d]	-
	FM	3.89[d]	-	-	254.4[d]	-
		3.86[e]	-	-	-	-
		3.885[f]	-	-	-	-
PtCo	This work					
	GGA(NM)	3.798*	3.634*	0.957*	252*	4.40*
	GGA(FM)	3.808*	3.732*	0.979*	216*	4.82*
	Experimental	3.810[j]	3.695[j]	0.971[j]	-	-
	Other calculations					
	NM	3.823[d]	3.641[d]	0.952[d]	250.5[d]	-
	FM	3.821[d]	3.703[d]	0.969[d]	229.4[d]	-
		3.810[e]	3.718[e]	0.976[e]	-	-
		3.809[f]	3.708[f]	0.973[f]	-	-
		3.806[h]	3.707[h]	0.979[h]	-	-
		3.746[i]	3.622[i]	0.967[i]	-	-
		3.819[g]	3.715[g]	0.973[g]	-	-
		3.800[k]	3.693[k]	0.972[k]	-	-
$PtCo_3$	This work					
	GGA(NM)	3.61*	-	-	252.8*	4.70*
	GGA(FM)	3.668*	-	-	209.6*	4.65*
	Experimental	3.664[l]	-	-	-	-
	Other calculations					
		3.672[b]	-	-	-	-
		3.666[c]	-	-	-	-
	NM	3.612[d]	-	-	299.0[d]	-
	FM	3.661[d]	-	-	259.6[d]	-
		3.66[e]	-	-	-	-
		3.654[f]	-	-	-	-

*Our calculation: [a]Ref. [75] exp, [b]Ref. [53] PP- PAW- GGA and MC, [c]Ref. [76] PAW-GGA , [d]Ref. [51] PP-GGA, [e]Ref. [42] PAW-GGA, [f]Ref. [8] PP-PAW, [j]Ref. [77] exp, [h]Ref. [24] PP-GGA, [i]Ref. [65] PP-LDA, [g]Ref. [65] PP-GGA, [k]Ref. [78] exp, [l]Ref. [79] Exp.

3.2. Electronic structure and magnetic Properties

Proportional stability can be discussed in detail by studying the electronic properties of the compound. To comprehend the electronic structure and magnetic features of Pt-Co binary materials, the band structure along selected

high-symmetry directions in the first Brillouin zone, the total density of states (TDOS), and partial density of states (PDOS) at equilibrium lattice constants have been calculated. Although the cohesive properties suggest that the nonmagnetic states could be synthesized experimentally. The TDOS of the studied compounds have been shown in Fig. 3(a). The foremost feature is the Fermi level lying at high DOS peaks, as also reported by Karoui *et al*. for paramagnetic PtCo, thereby promoting the instability of the nonmagnetic phase toward ferromagnetism [42].

Figs. 3(b and c) show the combined band structure and TDOS (for both spins) of Pt_3Co. For simplicity, and due to their similarity, the corresponding figures for PtCo and $PtCo_3$ are not shown. The valence and conduction bands exhibit significant overlay, with numerous bands crossing the Fermi level, indicating metallic behavior in all compounds. The noticeable asymmetric band distribution of spin-up and spin-down bands reflects the strong magnetic character of the Pt–Co binary compounds.

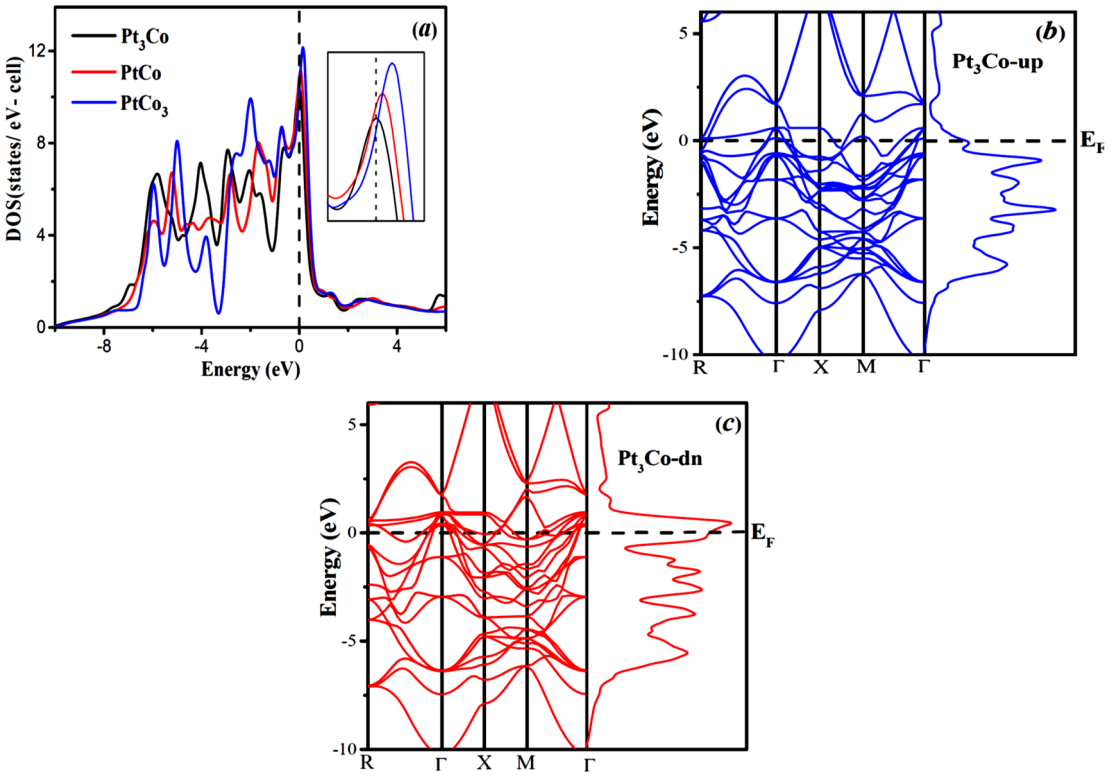

Figure 3. TDOS of Pt_3Co, PtCo and $PtCo_3$ compounds in NM states (a), band structure with the corresponding DOS of spin up (b) and spin down for Pt_3Co compound (c)

Figure 4 shows the PDOS for all compounds. It can be observed that the electronic states are strongly because of Pt-5d and Co-*3d* orbitals; and the contributions of *s* and *p* orbitals in the DOS are negligible compared to the *d* band contribution. Therefore, the Pt and Co-*d* states are the main origin of the absolute spin polarization. The bands crossing the Fermi level are chiefly composed of hybridized Pt-5*d* and Co-3*d* states. Table 3 reports the TDOS at the Fermi level N(EF), and the magnetic moment per atom. The overall magnetic moments for the investigated materials are 2.98, 4.5, and 5.66 (μB) for Pt_3Co, PtCo, and PtCo3, respectively. The results have been matched with the obtainable results [8, 24, 51, 53, 58, 82]. In addition, the degree of polarization, which is evaluated by the fractional difference between the two spin states at the Fermi level (E_F), is given below [80, 81].

$$P = \frac{n_{\uparrow}(E_F) - n_{\downarrow}(E_F)}{n_{\uparrow}(E_F) + n_{\downarrow}(E_F)} \tag{4}$$

where $n_{\uparrow}(E_F)$ *and* $n_{\downarrow}(E_F)$ are, respectively, the spin-up and spin-down DOS at the Fermi level.

The value of P discriminates the material type: P=0 corresponds to a paramagnetic state, while a finite value indicates antiferromagnetic nature. The obtained polarization values for all compounds are abridged in Table 3. It is worth mentioning that neither $n_{\uparrow}(E_F)$ nor $n_{\downarrow}(E_F)$ vanishes at E_F, resulting in a non-zero value of P, suggesting ferromagnetic systems. The electronic specific heat coefficients values are found out by means of the below equation:

$$\gamma_{th} = \pi^2 {k_B}^2 N(E_F)/3 \tag{5}$$

where k_B is the Boltzmann constant. The calculate values are 24.32, 25.08 and 23.08mJ/ mol^{-1} K^{-2} for Pt_3Co, PtCo and $PtCo_3$, respectively (Table 3).

Table 3. TDOS at N(E_F) (states/eV- cell), γ_{th} (mJ/mol. K^2), $n_\uparrow$ (E_F), $n_\downarrow$ (E_F) DOS at Fermi level for spin up and spin down, respectively, degree of polarization P %, and entire magnetic moment μ (in μB) for Pt_3Co, PtCo and $PtCo_3$.

System	N(E_F)	γ_{th}	μ	$n\uparrow(E_F)$	$n\downarrow(E_F)$	P %
Pt_3Co	10.32*	24.32*	Tot:2.98*;3.47[a];2.92[b];2.8[c];2.47[c] (Co:1.99, Pt:0.34)* (Co: 1.89, Pt: 0.24)[d]	1.54*	3.96*	-44*
PtCo	10.64*	25.08*	Tot:4.5*;4.31[e];2.38[f];2.26[j] (Co:1.91; Pt:0.41)* (Co: 1.96, Pt: 0.25)[j] (Co: 1.83, Pt: 0.37)[d] (Co:1.74; Pt:0.44)[f]	0.78*	3.67*	-64*
$PtCo_3$	9.79*	23.08*	Tot:5.66*;6.72[a];5.6[b] (Co:1.83; Pt:0.4)*	0.73*	4.19*	-70*

*Our calculation, [a]Ref. [53] PBE + U , [b]Ref.[8] PP- PAW, [c]Ref. [82] exp, [d]Ref. [83] SP-GGA, [e]Ref. [24], PP- PAW, [f]Ref. [58] PBE-GGA, [j]Ref. [51] PP.

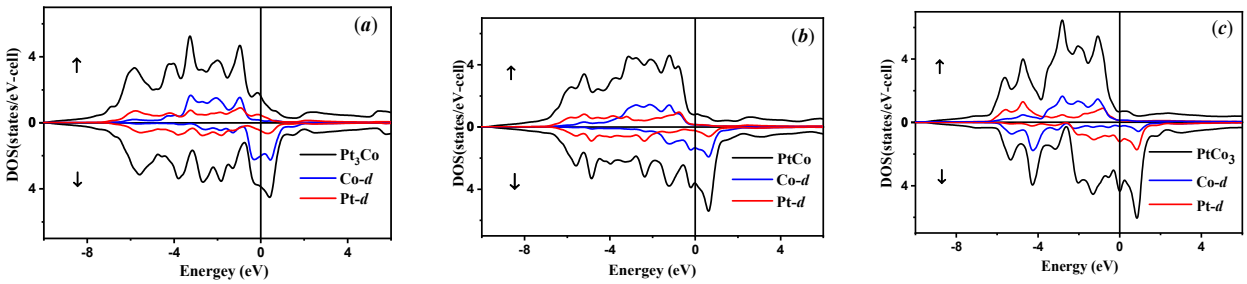

Figure 4. Spin polarized, TDOS and PDOS for Pt_3Co (a), PtCo (b), and $PtCo_3$ (c)

3.3. Single-crystal elastic properties

Recently, the study of elastic parameters has played a crucial role in materials science and engineering. The elastic constants C_{ij} reflect the mechanical response of crystals to applied external forces. In this section, we discuss the stability, ductility, anisotropy and bonding features of Pt-Co binary compounds. In the current investigation, the single-crystal elastic constants C_{ij} for the selected compounds have been evaluated using the IRelast program implemented in the WIEN2k package [66] with the PBE-GGA approximation. The attained values are tabulate in Table 4, we can observe that, for cubic structure, 3 independent elastic constants C_{11}, C_{12} and C_{44}, satisfy the Born mechanical stability criteria (C_{11}> 0, C_{44}> 0, $C_{11} + 2C_{12} > 0$, and C_{11}- C_{12} >0) and for tetragonal phase the six independent coefficient satisfy stability criteria (C_{11}> 0, C_{33}> 0, C_{44}> 0, C_{66}> 0, $(C_{11} - C_{12}) > 0$, $(C_{11} + C_{33} - 2C_{13}) > 0$ and $[2(C_{11} + C_{12}) + C_{33} + 4C_{13}] > 0$) [84].

Table 4. C_{ij} (GPa), B (GPa), G (GPa), E (GPa), B/G ratio, ν, and Hv for Pt_3Co, PtCo and $PtCo_3$

Compounds	C_{11}	C_{12}	C_{13}	C_{33}	C_{44}	C_{66}	**B**	G	E	B/G	ν	Hv
Pt_3Co	317.8*	172.5*	-	-	104.5*	-	220.9*	90.3*	241.8*	2.44*	0.31*	6.78*
	322[a]	218[a]			93.1[a]		252[a]					
							232.6[b]	93.6[b]	247.7[b]	2.48[b]	0.32[b]	
	321.2[c]	188.3[c]			117.9[c]						0.32[c]	
											0.33[d]	
PtCo ($L1_0$)	456.4*	149.4*	158.6*	305.5*	164.5*	102.5*	235.3*	132.2*	334.0*	1.77*	0.26*	14.7*
	323[a]	210[a]			87.4[a]		231[a]					
$PtCo_3(L1_2)$	302.1*	165.6*	-	-	152*	-	211.1*	110.2*	299.4*	1.90*	0.26*	11.6

*Our calculation: [a]Ref. [14] 2NN MEAM, [b]Ref. [74] PP- PAW- GGA, [c]Ref. [59] PP- PAW- GGA, [d]Ref. [100] PP- PAW- GGA.

The two elastic constants C_{11} and C_{33} describe the stiffness along the crystallographic *a (or b)* and *c* axes, respectively. For PtCo in tetragonal phase $L1_0$, we can constat that the C_{11}>C_{33}, the compound resists deformation along the *a* (or *b*)-axis more strongly than the *c*-axis (is additional compressible along the c-axis than that of along *a*- and *b*-axis), demonstrating that the bonds are stronger along <100> and <010> directions as comparation to bonds along <001> direction. C_{44} reflects the resistance to shear in the (100) plane, and C_{66} measures the resistance to shear along <110> orientation. Indicating the material is harder to shear along c-axis than in-plane.

We can see that C_{11} and C_{12} are closer in cubic compounds, indicating that the two materials have the same response to uniaxial compression and lateral deformation, whereas C_{44} ($PtCo_3$)> C_{44} (Pt_3Co) indicates $PtCo_3$ possesses superior resistance to shear deformation. On the contrary, both compounds resist longitudinal deformation more than shape deformation (C11 > C12 > C_{44}).

The comparison with the previously reported values shows a good agreement with Ref [14,49] for Pt_3Co compound and a considerable deviation for PtCo [14]. To our knowledge, no data are available in the literature for PtCo3-L12, so the results of the present investigation can serve as a guide for future investigations.

3.4. Mechanical properties and dynamic stability

The Voigt–Reuss–Hill (VRH) approximation is applied to estimate the polycrystalline mechanical parameters of materials by averaging the Voigt (upper**)** and the Reuss (lower) limits [85-87]. The polycrystalline bulk modulus (*B*) denotes resistance to volume change with uniform compression**)** and shear modulus (*G*) refers resistance to shape change, shear deformation**;** for isotropic aggregates are $B = (B_V + B_R)/2$ and $G = G_V + G_R/2$, repectively. B_V (B_R) and G_V (G_R) represent the Voigt's (Reuss's) bulk modulus and the Voigt's (Reuss's) shear modulus respectively. According to Refs. [85] and [86], Voigt and Reuss modulus are derived from the independent single-crystal constants C_{ij}.

The computed elastic modulus B and G of Pt_3Co, PtCo and $PtCo_3$ are enumerated in Table 4. Table 4 shows accord with the bulk modulus values obtained from the equation of state. This serves as proof of the consistency and accurateness of the elastic constants we've calculated for these compounds.

In accordance with our analysis, PtCo-L10 has a large bulk modulus, indicating high incompressibility. The shear modulus *G* (modulus of rigidity*)* of the studied compounds is in order: PtCo > Pt_3Co >$PtCo_3$, thus the tetragonal PtCo resists more the shear deformation (shape change without volume change) than the cubic compounds. Hence, we can predict with strong directional covalent bonds in PtCo.

The Young's modulus (*E*) and Poisson's ratio (ν) have been given below:

$$E = \frac{9BG}{3B+G} \tag{6}$$

$$\nu = \frac{3B-2G}{2(3B+G)} \tag{7}$$

The Young's modulus value of PtCo is greater than that of $PtCo_3$ and Pt_3Co, consequently, PtCo is stiffer than other compounds. The Young modulus describes the stickness of the compound [88]. Furthermore, ductility of Pt-Co binary compounds is determined based on the Pugh's criteria (*B*/*G*) [89] (critical value of Pugh's criteria is equal to 1.75: ductility >brittleness), the Pugh's criteria are larger than 1.75 for the selected materials, indicating the ductility of compounds, the PtCo behave with low ductility, *B*/*G* is 1.77, whereas Pt_3Co behave with high ductility, B/G is 2.44. Li *et al* [49, 74] have found that when *B*/*G* > 1.75, it suggests that Pt_3Co is ductile. According to Poisson's ratio values, if ν> 0.26, the material performs in a ductile manner, else it is brittle [90]. Hence, Pt_3Co is ductile and PtCo possesses a low ductility *i.e.* is brittle. According to Pettifor the Cauchy pressure, for ductile materials with metallic bonding, are positive, it's the case of the studied cubic compounds (Pt_3Co and $PtCo_3$, Table 5). The more negative the Cauchy pressure, the more directional covalent or ionic bonds, were directional bonding leads to brittleness. The positive/negative Cauchy pressure C_{12}-C_{66}/C_{13}-C_{44} suggests the mixture of bonding and weak of ductility of tetragonal PtCo material. The Vickers hardness (H_V) is applied to guesstimate the resistance of the Pt-Co binary materials to plastic deformation. the formula used to calculate H_V [91] is:

$$H_v = 2\left(\frac{G^3}{B^2}\right)^{0.585} - 3 \tag{8}$$

The evaluated hardness is itemized in Table 4. Hence, Pt_3Co has the lowermost H_V owing to its relative ductility and metallic bonds. whereas, the PtCo compound has the maximum Hv due to the stronger covalent bonding.

The longitudinal and transverse acoustic velocities v_l ($v_l = [(3B + 4G)/3\rho]^{\frac{1}{2}}$) and v_t ($v_t = G/\rho$), respectively, are determined as well as the mean sound velocity v_m ($v_m = \left[\frac{1}{3}\left(\frac{1}{{v_l}^3} + \frac{2}{v_t^3}\right)\right]^{\frac{-1}{3}}$), in order to calculate the Debye temperatur Θ_D using Refs. [92, 93]:

$$\theta_D = \frac{h}{k_B}\left[\left(\frac{3n}{4\pi}\right)\frac{N_A}{M}\right]^{\frac{1}{3}} v_m \tag{9}$$

where k_B, h, and ρ denote Boltzmann's constant, Plank's constant, and the density, correspondingly. N_A, M and n refer the Avogadro's number, the molecular weight and the number of atoms in the molecule respectively. In addition, the approximate melting temperature of the selected compounds has been evaluated using the succeeding empirical equation [94]:

$$T_m = [553\ \mathrm{K} + (5.91\ \mathrm{K/GPa})C_{11}] \pm 300\mathrm{K} \tag{10}$$

The evaluated values of the acoustic velocities (v_t, v_l and v_m**)**, Debye temperature θ_D and melting temperature T_m have been provided in Table 5 for the selected Pt_3Co, PtCo and $PtCo_3$. The values v_t, v_l *and* v_m for Pt_3Co are coincide with theoretical data [49]. The longitudinal velocities of sound in all considered alloys is considerably greater than in the transverse velocities. Out of these, $PtCo_3$ supports the highest supremely average sound velocity ($v_m = 3294.96$ m/s**)**.

Table 5. C_P=C_{12}–C_{44} for cubic, (C_{12}–C_{66})/(C_{13}–C_{44}) ratio for tetragonal structures, A^U, ν, V_l (in m/s), V_t (in m/s), V_m (in m/s), θ_D (in K) and T_m (K) for Pt_3Co, PtCo and $PtCo_3$

Compounds	C_{12}-C_{44}	C_{12}-C_{66}/C_{13}-C_{44}	A^U	V_l	V_t	V_m	$\boldsymbol{\theta_D}$	T_m∓300
Pt_3Co	68	-	0.15*	4317*	2221*	2487*	302.9*	2431*
			0.4[a]	4421[a]	2263[a]	2535[a]	308.6[a]	
			0.46[b]					
PtCo	-	47/-6	0.39*	5040*	2856*	2009*	402.0*	3176*
$PtCo_3$	14	-	0.81*	5331*	2958*	3295*	425.4*	2338*

*Our calculation: [a]Ref. [74] PP- PAW- GGA, [b]Ref. [49] PP- PAW- GGA.

A larger θ_D designates an augmented thermal conductivity [95] signifying that the $PtCo_3$ is anticipated to show a relatively greater thermal conductivity matched with the other materials. In [74], Li *et al.* described a Debye temperature (θ_D) of 308.6 K for Pt_3Co, which discloses a concordance to the achieved calculated value of 302.9 K.

From Table 5, it can be observed that all compounds melt at high temperatures. According to the experimental Pt-Co phase illustration [70] and our T_m values are over estimate. The Pt-Co system has, at low temperatures, an ordered fcc structure and a disordered one at high temperatures. The order-disorder transition temperatures were experimentally reported to be 1000, 840 and 1100 K for Pt_3Co, $PtCo_3$ and for PtCo, respectively [96]. The chemical ordering is attributed to the magnetic moment of Pt and Co atoms [97].

In addition, in the (VRH) scheme the material's anisotropy is also given via the universal anisotropic index A^U(A^U=5G_V/G_R+(B_V/B_R)–6) [98]. The evaluated results of A^U for Pt-Co intermetallic materials are gathered in Table 5. The deviation of all A^U indexes from zero (A^U = 0 for an isotropic crystal) [99] indicates the anisotropic behavior of the three compounds, with $PtCo_3$ exhibiting a relatively greater degree of elastic anisotropy.

The 3D-representation of the dependence of the elastic modules on the crystallographic direction is a modern method applied to estimate the degree of elastic anisotropy in materials. Fig. 5 depicts the 3D-representation of the Young's modulus for Pt-Co binary materials. It is clearly seen that there is a small nonconformity from spherical shape suggesting modest degree of elastic anisotropy for all compounds. In materials sciences, the spherical 3D surface shape of Young's modulus corresponds to isotropic materials.

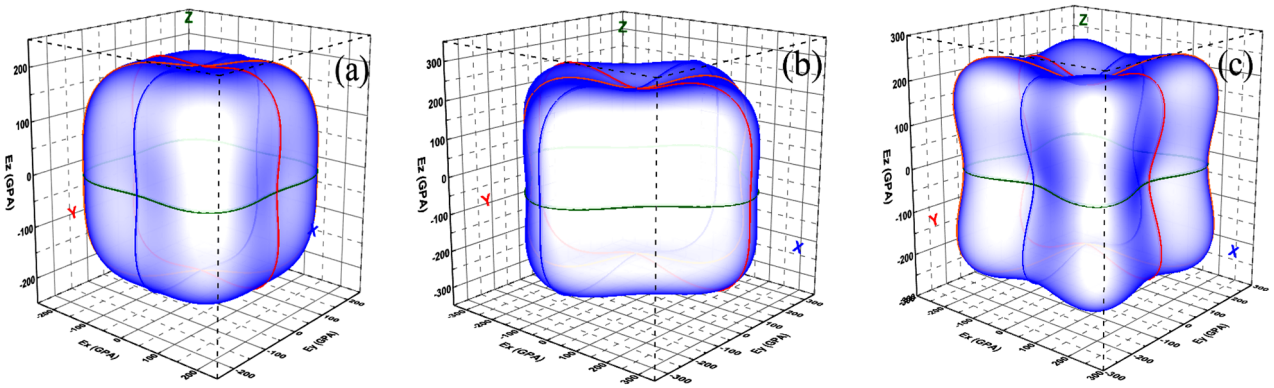

Figure 5. 3D-presentation of the surface related to Young's modulus (Y) for: Pt_3Co (a), PtCo (b),: $PtCo_3$(c) compounds

3.5. Thermal properties

In this subdivision, the thermodynamics features of ferromagnetic Pt-Co binary intermetallics materials are explored versus temperature (0-1000 K) and pressure (0-30). The main values of bulk modulus *B*, heat capacities C_V and C_P, Debye temperature θ_D, thermal expansion coefficient α, the Grüneisen parameter γ_G and entropy *S* have been tabulated in Table 6 and some of them have been shown in Fig. 6.

Table 6. Temperature and pressure dependent *B* (in GPa), C_V and C_P (in J/mol. K), α (10^5/K), θ_D (K), γ_G and *S* (in J/mol. K)

Compounds	T	P	B	C_V	C_P	*A*	θ_D	γ_G	S
Pt_3Co	0	0	229.3*	0*	0*	0*	372.1*	3.1*	0*
		30	388.5*	0*	0*	0*	475.2*	2.0*	0*
	300	0	207.1*	92.8*	96.4*	4.0*	363.4*	3.2*	117.4*
		30	380.4*	88.3*	89.2*	1.4*	472.9*	2.0*	93.5*
	900	0	121.0*	99.1*	131.5*	8.9*	319.6*	4.0*	236.6*
		30	349.6*	98.4*	102.0*	1.8*	462.7*	2.1*	200.0*
PtCo	0	0	215.6*	0*	0*	0*	405.2*	2.77*	0*
		30	366.7*	0*	0*	0*	509.5*	1.8*	0*
	300	0	195.7*	45.8*	47.4*	4.1*	396.6*	2.88*	54.7*
		30	359.7*	43.4*	43.8*	1.5*	507.0*	1.8*	43.7*

Compounds	T	P	B	C_V	C_P	A	θ_D	γ_G	S
	900	0	120.7*	49.5*	63.1*	8.6*	355.3*	3.5*	113.0*
		30	331.4*	49.1*	50.7*	1.9*	497.6*	1.8*	96.5*
$PtCo_3$	0	0	208.9*	0*	0*	0*	452.2*	2.3*	0*
		30	339.9*	0*	0*	0*	566.73*	1.8*	0*
	300	0	198.3*	89.5*	91.8*	3.5*	445.4*	2.3*	98.8*
		30	333.9*	84.1*	84.9*	1.7*	563.8*	1.8*	78.3*
	900	0	136.9*	98.5*	108.9*	5.1*	451.7*	2.2*	202.4*
		30	271.6*	97.5*	100.5*	2.0*	599.5*	1.6*	174.6*

* Our calculation.

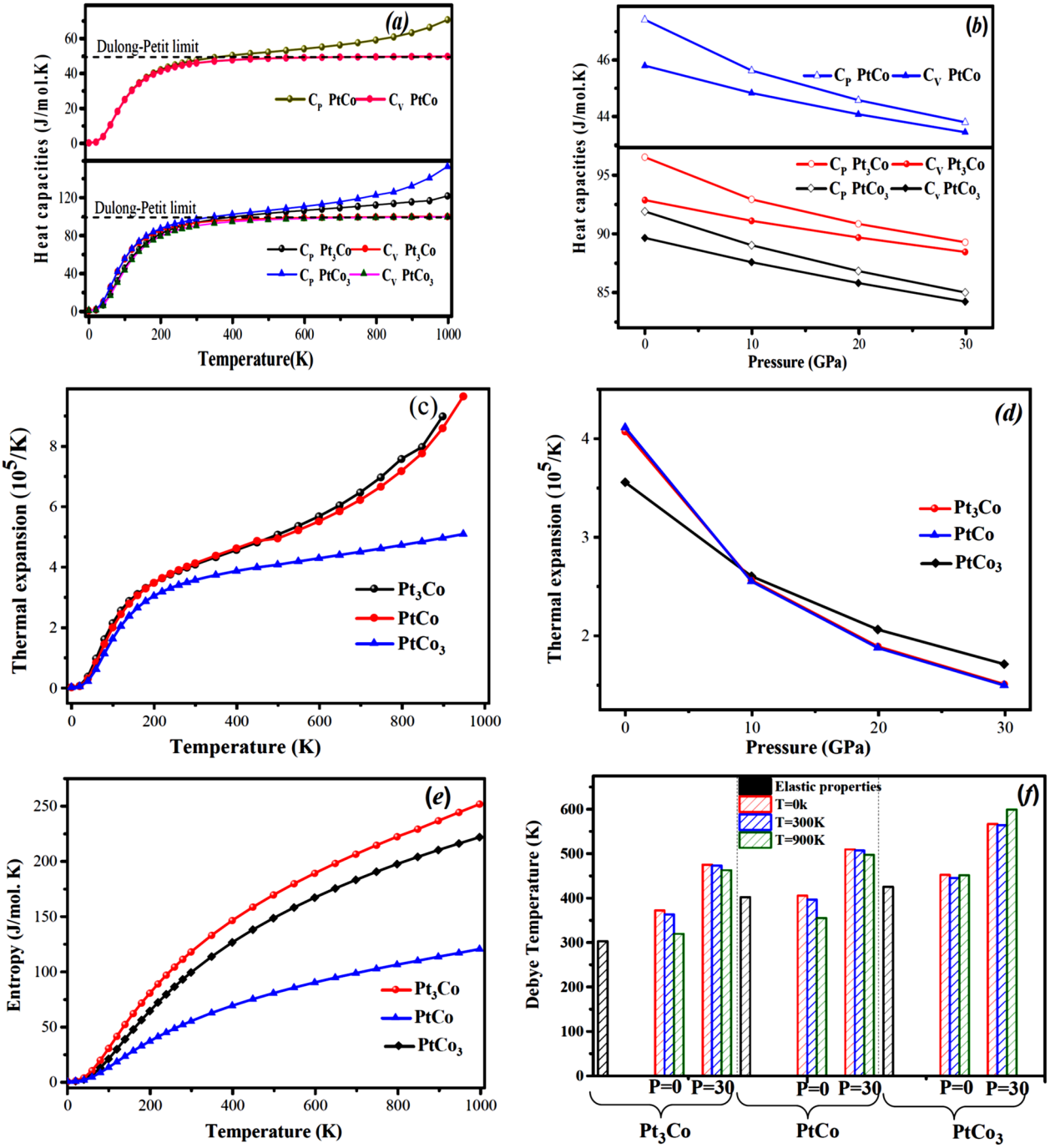

Figure 6. Temperature and pressure dependent thermodynamic parameters of Pt-Co binary materials: (a, b) C_P and C_V, (c, d) α and (e) S

Based on the quasi-harmonic Debye model and the unit cell energies E(V), obtained in the first subsection, as input data, the GIBBS code [101] is used to illustrate both temperature and pressure influences. A thorough explanation of this process is given in the literature [101]. At ambient temperature and zero pressure (P=0), the values of C_V (C_P)

are 89.5 (91.8) and 92.8 (96.4) $Jmol^{-1}$ K^{-1} for $PtCo_3$, and Pt_3Co, correspondingly, with values impending zero at low temperatures. These values are 45.8 (47.4) $Jmol^{-1}$ K^{-1}, respectively, for CoPt. From Fig. 6(a), it can be understood that both quantities upsurge with T^3 at temperatures below 400 K.Beyond this range, the anharmonic things on the heat capacity C_V become insignificant for all compounds. As a result, C_V reaches a constant value, nearby to the Dulong–Petit limit [102] (C_V=3nR = 25×n J/mol K, n: number of atoms in the unit cell), whereas C_P undergoes to rise with temperature. At a given temperature, both C_P and C_V decrease with growing pressure. The thermal expansion coefficient α has the maximum values at zero pressure and significantly drops as pressure rises at a constant temperature, showcasing the compressive nature of solids. Whereas α augment rapidly with temperature in all range of T, at elevated T the speed of increase decreases mostly for $PtCo_3$ compound (Fig. 6(c)). The thermal expansion coefficient (α) attains its highest values at zero pressure and reduces significantly as pressure increases at constant temperature, reflecting the compressive nature of solids. Although α increases rapidly with temperature across the entire range of T, the rate of increase slows at higher temperatures, most notably for the $PtCo_3$ compound (Fig. 6(d)). In addition, α for Pt_3Co and PtCo are very closer and higher than that of $PtCo_3$. To assess the order and disorder in the Pt-Co alloy based on temperature and pressure, the changes in entropy have been exposed in Fig. 6(e). It can be perceived that the entropy approaches zero at 0 K and 0 GPa, then increases with rising temperature at constant pressure. The increase in entropy indicates a growing degree of disorder within the Pt–Co alloy as the temperature rises, with this effect being particularly considerable for the Pt_3Co compound. From Table 6, we can see that both parameters B and θ_D increase (decrease) with pressure (temperature). At static states (T = 0K, P = 0 GPa), the calculated θ_D for Pt_3Co, PtCo and $PtCo_3$, are 372.1, 405.2 and 452.2 K, respectively. In Table 5, the attained θ_D values from elastic constant C_{ij} are 302.9, 402 and 425.5 K for Pt_3Co, PtCo and $PtCo_3$, respectively, and the concordance for all the studied compounds is clearly seen (Fig. 6(f)). This accord is also observed in calculated bulk modulus (Tables 4 and 6). As for the Grüneisen parameter γ_G, it rises with temperature and diminishes with pressure.

4. CONCLUSIONS

In the present investigation, DFT-based computations were conducted to examine the structural, electronic, mechanical, and thermodynamic features of the intermetallics Pt-Co. The evaluated lattice parameters show strong agreement with obtainable experimental data and preceding theoretical data. The negative formation enthalpies confirm that Pt_3Co, PtCo, and $PtCo_3$ can be synthesized and remain chemically stable in all considered structures. The investigation of the electronic band structure, DOS, and PDOS reveals that the Co–*3d* and Pt–*5d* states contribute significantly to the total DOS through strong hybridization. The noticeable asymmetry between spin up and spin down states in all compounds indicates significant magnetization. In particular, Pt_3Co, PtCo and $PtCo_3$ exhibit strong magnetic behavior because of the large spin polarization near the Fermi level. Mechanical property calculations further demonstrate the elastic stability of these compounds. Pugh's criterion, Poisson's ratio, and Cauchy pressure indicate that both Pt_3Co and $PtCo_3$ are ductile with a metallic character. In contrast, PtCo possesses a mixed bonding nature (metallic and directional covalent) and exhibits the lowest ductility (B/G=1.77), making it the hardest compound. The evaluation of the elastic anisotropy (A^U and the 3D surface of Young's modulus) suggests a relatively low degree of anisotropy for all compounds. Thermodynamic features, including the bulk modulus (B), thermal expansion coefficient (α), heat capacities (C_V, C_P), entropy (S), and Debye temperature (θ_D), were systematically examined with the quasi-harmonic Debye model, highlighting their dependence on both temperature and pressure. Overall, the PtCo alloy exhibits a significant magnetic moment, making it a promising entrant for a variability of magnetic and spintronic utilizations.

Acknowledgments

D. Singh expresses his sincere gratitude to the Department of Science & Technology, New Delhi for support under the DST-PURSE Scheme (SR/PURSE/2024/230) of V.B.S. Purvanchal University Jaunpur and to the Council of Science & Technology, U.P. (CSTUP), Lucknow for funding under research project (UP-CST/E&T/D-1235, PID-6261).

Declarations

Ethics approval and consent to participate

Consent for publication: All authors approve of the ethics.

Funding: This research did not receive any specific grant from funding agencies in the public, commercial, or not-for-profit sectors.

Competing interests: The authors have no relevant financial or non-financial interests to disclose.

Author's contributions: H. Grimed: Investigation, Resources, Writing-Original draft. **D. Sayad:** Conceptualization. **R. Boulechfar:** Formal Analysis, Supervision, Writing-Original draft. **H. Bensadalla:** Methodology. **F. Semari:** Formal Analysis, Visualization. **Y. Khenioui:** Supervision, Resources. **H. Meradji, R. Khenata:** Supervision, Writing-Reviewing and Editing. **M. Boudjelal:** Validation, Investigation. **S. Ghemid:** Software. **D. Singh:** Visualization, Writing-Original draft

Availability of data and materials: Not applicable

ORCID

R. Boulechfar, https://orcid.org/0009-0006-2015-739X; **F. Semari,** https://orcid.org/0009-0001-0778-9118; **D. Sayad,** https://orcid.org/0000-0002-8179-8127; **M. Boudjelal,** https://orcid.org/0000-0001-5772-1878; **H. Meradji,** https://orcid.org/0000-0002-3359-3725; **D. Singh,** https://orcid.org/0000-0002-3011-2375; **R. Khenata,** https://orcid.org/0000-0002-5573-1711

REFERENCES

[1] B.S. Mun, M. Watanabe, M. Rossi, V. Stamenkovic, N.M. Markovic, P.N. Ross, J. Chem. Phys. **123**, 204717 (2005). https://doi.org/10.1063/1.2126662
[2] Z.M. Liu, L.L. Ma, J. Zhang, K. Hongsirikarn, and J.G. Goodwin, Catal. Rev. **55**, 255 (2013). https://doi.org/10.1080/01614940.2013.795455
[3] N.A. Frey, and S. Sun, *Inorganic Nanoparticles: Synthesis, Application, and Perspectives*, (CRC Press, Boca Raton, 2010), pp. 33–68.
[4] J.M. Montejano-Carrizales, F. Aguilera-Granja, C. Goyhenex, V. Pierron-Bohnes, J.L. Morán-López, J. Magn. Magn. Mater. **355**, 215–224 (2014). https://doi.org/10.1016/j.jmmm.2013.10.035
[5] N.L. Lethole, P. Mukumba, and G. Makaka, J. Alloys Compd. **565**, 170298 (2023). https://doi.org/10.1016/j.jmmm.2022.170298
[6] D. Weller, A. Moser, L. Folks, M.E. Best, W. Lee, *et al*., IEEE Trans. Magn. **36**, 10 (2000). https://doi.org/10.1109/20.824418
[7] D.J. Sellmyer, M. Yu, R.A. Thomas, Y. Liu, and R.D. Kirby, Phys. Low-Dimens. Struct. **1–2**, 155–165 (1998).
[8] D. Kim, J.E. Saal, L. Zhou, S. Shang, Y. Du, Z.-K. Liu, Calphad, **35**, 323 (2011). https://doi.org/10.1016/j.calphad.2011.04.005
[9] U.A. Paulus, A. Wokaun, G.G. Scherer, T.J. Schmidt, V. Stamenkovic, V. Radmilovic, N.M. Markovic, and P.N. Ross, Electrochim. Acta, **47**, 3787 (2002). https://doi.org/10.1016/s0013-4686(02)00349-3
[10] M.T.M. Koper, Surf. Sci. **548**, 1–3 (2004). https://doi.org/10.1016/j.susc.2003.10.045
[11] W. Yu, M.D. Porosoff, and J.G. Chen, Chem. Rev. **112**, 5780 (2012). https://doi.org/10.1021/cr300096b
[12] V.R. Stamenkovic, B.S. Mun, M. Arenz, K.J.J. Mayrhofer, C.A. Lucas, G. Wang, P.N. Ross, *et al*., Nat. Mater. **6**, 241 (2007). https://doi.org/10.1038/nmat1840
[13] B.N. Grgur, G. Zhuang, N.M. Markovic, and P.N. Ross, J. Phys. Chem. B, **101**, 3910 (1997). https://doi.org/10.1021/jp9704168
[14] J.-S. Kim, D. Seol, J. Ji, H.-S. Jang, Y. Kim, and B.-J. Lee, Curr. Appl. Phys. **59**, 131-141 (2017).
[15] I. Galanakis, M. Alouani, and H. Dreyssé, J. Magn. Magn. Mater. **320**, 221(2002). https://doi.org/10.1016/s0921-4526(02)00687-7
[16] K. Aledealat, B. Aladerah, A. Obeidat, M. Gharaibeh, Heliyon, **7**, e08639 (2021). https://doi.org/10.1016/j.heliyon.2021.e08639
[17] M. Futamoto, M. Nkamura, M. Ohtake, N. Inaba, and T. Shimotsu, AIP Adv. **6**, 085302 (2016). https://doi.org/10.1063/1.4960554
[18] K.M. Krishnan, C. Nelson, C.J. Echer, R.F.C. Farrow, R.F. Marks, and A.J. Kellock, J. Appl. Phys. **83**, 6810 (1998). https://doi.org/10.1063/1.367815
[19] S.C. Tsang, C.H. Yu, H. Tang, H. He, V. Castelletto, I.W. Hamley, T. Narayanan, *et al*., Chem. Mater. **20**, 4554 (2008). https://doi.org/10.1021/cm801068j
[20] Y. Wang, X. Zhang, Y. Liu, Y. Jiang, Y. Zhang, and J. Yang, J. Mater. Sci.: Mater. Electron. **70**, 528 (2014).
[21] M. Neamtu, C. Nadejde, V.D. Hodoroaba, R.J. Schneider, L. Verestiuc, and U. Panne, Sci. Rep. **8**, 6278 (2018). https://doi.org/10.1038/s41598-018-24721-4
[22] T.S. Rodrigues, A.G.M. da Silva, and P.H.C. Camargo, J. Mater. Chem. A, **7**, 5857 (2019). https://doi.org/10.1039/c9ta00074g
[23] L.M. Rossi, N.J.S. Costa, F.P. Silva, and R. Wojcieszak, Green Chem. **16**, 2906 (2014). https://doi.org/10.1039/c4gc00164h
[24] A.M. Alssad, A.A. Ahmed, H.A. Qattous, Heliyon, **5**, e02433 (2019). https://doi.org/10.1016/j.heliyon.2019.e02433
[25] A. Obeidat, B. Aladerah, M.-K. Qaseer, J. Alloys Compd. **559**, 169501 (2022). https://doi.org/10.1016/j.jmmm.2022.169501
[26] H. Okamoto, J. Phase Equilib. Diffus. **40**, 743 (2019). https://doi.org/10.1007/s11669-019-00760-w
[27] J. Cui, Y. Zeng, Q. Zheng, Q. Peng, F. Yu, X. Wang, N. Xie, *et al*., Fuel, **142**, 292 (2025). https://doi.org/10.1016/j.ijhydene.2025.05.394
[28] R. Wu, J. Zuo, L. Zhao, Z. Zhu, Q. Li, X. Niu, and J.S. Chen, Chem. Commun. **61**, 5742 (2025). https://doi.org/10.1039/d5cc00736d
[29] Y.-L. Mai, X.-S. Xie, Z.-D. Wang, C.-F. Yan, and G.-H. Liu, Trans. Nonferrous Met. Soc. China, **50**, 114–121 (2022).
[30] H. Li, D. Wei, C. Shi, Q. Long, L. Zhou, H. Jin, J. Yu, *et al*., J. Alloys Compd. **985**, 119089 (2025). https://doi.org/10.1016/j.jelechem.2025.119089
[31] J. Shen, C. Chen, L. Song, L. Zhong, K. Shan, Y. Guo, W. Zhan, *et al*., Wang, Appl. Surf. Sci. **379**, 133066 (2025). https://doi.org/10.1016/j.fuel.2024.133066
[32] Z. Qin, L. Wu, R. He, Z. Meng, J. Pan, and J. Zeng, Appl. Surf. Sci. **475**, 143675 (2024). https://doi.org/10.1016/j.electacta.2023.143675
[33] H. Wang, J. Liu, K. Du, X. Wang, X. Li, Y. Liu, C. Min, *at al*., J. Power Sources, 616, 235127 (2024). https://doi.org/10.1016/j.jpowsour.2024.235127
[34] J. Zou, Y. Du, R. Fang, X. Duan, Y. Liu, J. Mao, L. Yu, *et al*., Fuel, **307**, 121794 (2022). https://doi.org/10.1016/j.fuel.2021.121794
[35] S. Wang, W. Xu, Y. Zhu, Q. Luo, C. Zhang, S. Tang, and Y. Du, J. Mater. Sci. **13**, 827 (2020).
[36] C. Luo, K. Wan, J. Wang, B. Li, D. Yang, P. Ming, and C. Zhang, Renew. Sustain. Energy Rev. **679**, 165 (2025). https://doi.org/10.1016/j.jcis.2024.10.063
[37] D. Fu, Z. Hu, J. Xun, X. Yu, L. Wang, S. Zeng, and F. Li, Fuel, **396**, 135250 (2025). https://doi.org/10.1016/j.fuel.2025.135250
[38] B. Ravichandran, N. Narayanan, H. Liu, W. Zhang, N. Bhuvanendran, and H. Su, J. Power Sources, **402**, 136040 (2025). https://doi.org/10.1016/j.fuel.2025.136040
[39] V. Domin, M. Prokop, T. Bystron, M. Gatalo, L. Pavko, N. Hodnik, B.F. Gomes, *et al*., Appl. Catal. B: Environ. **536**, 146707 (2025). https://doi.org/10.1016/j.electacta.2025.146707
[40] M. Kim, H.E. Bae, J. Song, T.B.N. Huynh, T.T. Pham, S.K. Cho,T. Lim, *et al*., Curr. Opin. Electrochem. **52**, 101934 (2025). https://doi.org/10.1016/j.mtener.2025.101934
[41] U. Guevara, R. López, J. Blanco, and J. Núñez, Mater. Res. Express, **6**, 096514 (2019). https://doi.org/10.1088/2053-1591/ab2c50
[42] S. Karoui, H. Amara, B. Legrand, and F. Ducastelle, J. Phys.: Condens. Matter, **25**, 056005 (2013). https://doi.org/10.1088/0953-8984/25/5/056005
[43] X. Gonze, J.-M. Beuken, R. Caracas, F. Detraux, M. Fuchs, G.-M. Rignanese, L. Sindic, *et al*., Comput. Mater. Sci. **25**, 478 (2002). https://doi.org/10.1016/s0927-0256(02)00325-7
[44] R. Boulechfar, Y. Khenioui, S. Drablia, H. Meradji, M. Abu-Jafar, S. Bin Omran, *et al*., Solid State Commun. **273**, 23 (2018). https://doi.org/10.1016/j.ssc.2018.02.005

[45] A.T. Khodja, R. Boulechfar, H. Meradji, Y. Akeb, R. Chemam, S. Ghemid, and X. Wang, Solid State Sci. **100**, 107651 (2020). https://doi.org/10.1016/j.jmgm.2020.107651
[46] A. Front, B. Legrand, G. Tréglia, C. Mottet, Surf. Sci. **679**, 128 (2019). https://doi.org/10.1016/j.susc.2018.08.024
[47] J.P. Perdew, and Y. Wang, Phys. Rev. B, **45**, 13244 (1992). https://doi.org/10.1103/physrevb.98.079904
[48] R.V. Chepulskii, and W.H. Butler, Phys. Rev. B, **86**, 155401 (2012). https://doi.org/10.1103/physrevb.86.155401
[49] Z.-B. Li, K. Xiong, C.-C. Jin, Y.-J. Sun, B.-W. Wang, S.-M. Zhang, J.-J. He, *et al*., Rare Met. **40**, 1208 (2021). https://doi.org/10.1007/s12598-020-01656-2
[50] J.P. Perdew, K. Burke, M. Ernzerhof, Phys. Rev. Lett. **77**, 3865 (1996). https://doi.org/10.1103/physrevlett.78.1396
[51] L. Zosiak, C. Goyhenex, R. Kozubski, and G. Tréglia, J. Phys.: Condens. Matter, **27**, 455503 (2015). https://doi.org/10.1088/0953-8984/27/45/455503
[52] S.-M. Zhang, K. Xiong, C.-C. Jin, Z.-B. Li, J.-J. He, and Y. Mao, Rare Met. **40**, 1020 (2021). https://doi.org/10.1007/s12598-020-01651-7
[53] K. Aledealat, B. Aladerah, and A. Obeidat, J. Alloys Compd. **363**, 115112 (2023). https://doi.org/10.1016/j.ssc.2023.115112
[54] M.A. Rahman, K. Mousumi, M.L. Ali, R. Khatun, M.Z. Rahman, S.S. Hasan, W. Hasan, *et al*., Results Phys. **44**, 106141 (2023). https://doi.org/10.1016/j.rinp.2022.106141
[55] M.N. Sadat, M.A. Rahman, D.C. Roy, M.A. Rahman, M.Z. Hasan, I. Ahmad, S. Chowdhury, *et al*., Physica B, **672**, 415402 (2024). https://doi.org/10.1016/j.physb.2023.415402
[56] Z. Wei, Y. Xie, Y. Xiao, J. Chen, J. Xue, N. Qu, and J. Zhu, J. Mater. Res. 1–11 (2025). https://doi.org/10.1557/s43578-025-01596-6
[57] P. Rani, M.K. Kashyap, R. Singla, J. Thakur, and A.H. Reshak, J. Alloys Compd. **835**, 155325 (2020). https://doi.org/10.1016/j.jallcom.2020.155325
[58] M. Islam, M.S.I. Sarker, T. Nakamura, M.K.R. Khan, F.A. Khan, M.A. Islam, and S. Sato, Mater. Chem. Phys. **269**, 124727 (2021). https://doi.org/10.1016/j.matchemphys.2021.124727
[59] Z. Zine, N. Meftah, Phys. Solid State, **66**, 416–423 (2024). https://doi.org/10.1134/s1063783424601115
[60] Z. Zine, N. Meftah, and B. Daoudi, Solid State Commun. **396**, 115769 (2025). https://doi.org/10.1016/j.ssc.2024.115769
[61] S. Imada, T. Muro, T. Shishidou, S. Suga, H. Maruyama, K. Kobayashi, and T. Kanomata, Phys. Rev. B, **59**, 8752 (1999). https://doi.org/10.1016/s0921-4526(97)00234-2
[62] J.M. Sanchez, J.L. Moran-Lopez, C. Leroux, and M.C. Cadeville, J. Phys. C: Solid State Phys. **21**, L1091–L1096 (1988). https://doi.org/10.1088/0022-3719/21/33/004
[63] J.M. MacLaren, R.R. Duplessis, R.A. Stern, and S. Willoughby, J. Appl. Phys. **41**, 4374 (2005). https://doi.org/10.1109/tmag.2005.854755
[64] A. Kootte, C. Haas, R.A. de Groot, J. Phys. : Condens. Matter, **3**, 1133 (1991). https://doi.org/10.1088/0953-8984/3/9/009
[65] A. Alam, B. Kraczek, D.D. Johnson, Phys. Rev. B, **82**, 024435 (2010). https://doi.org/10.1103/physrevb.82.024435
[66] P. Blaha, K. Schwarz, F. Tran, R. Laskowski, G.K.H. Madsen, and L.D. Marks, J. Chem. Phys. **152**, 074101 (2020). https://doi.org/10.1063/1.5143061
[67] O.K. Andersen, Phys. Rev. B, **12**, 3060 (1975). https://doi.org/10.1103/physrevb.12.3060
[68] J.P. Perdew, J.A. Chevary, S.H. Vosko, K.A. Jackson, M.R. Pederson, D.J. Singh, and C. Fiolhais, Phys. Rev. B, **46**, 6671 (1992). https://doi.org/10.1103/physrevb.46.6671
[69] F.D. Murnaghan, Proc. Natl. Acad. Sci. USA, **30**, 244 (1944). https://doi.org/10.1073/pnas.30.9.244
[70] R.G. Hennig, A.E. Carlsson, K.F. Kelton, and C.L. Henley, Phys. Rev. **71**, 100 (2005). https://doi.org/10.1103/physrevb.71.144103
[71] D. Zhou, J. Liu, S. Xu, and P. Peng, Comput. Mater. Sci. **51**, 409 (2012). https://doi.org/10.1016/j.commatsci.2011.07.012
[72] D. Zhou, J. Liu, S. Xu, and P. Peng, Comput. Mater. Sci. **86**, 24 (2014). https://doi.org/10.1016/j.commatsci.2014.01.007
[73] R. Hultgren, P.D. Desai, D.T. Hawkins, M. Gleiser, and K.K. Kelley, *Selected Values of the Thermodynamic Properties of Binary Alloys*, ASM, Metals Park, OH, 1973.
[74] Z. Li, K. Xiong, Y. Sun, C. Jin, S. Zhang, J. He, and Y. Mao, Comput. Condens. Matter, **23**, e00462 (2020). https://doi.org/10.1016/j.cocom.2020.e00462
[75] W.B. Pearson, *A Handbook of Lattice Spacings and Structures of Metals and Alloys*, (Pergamon Press, Oxford, 1964).
[76] Shuttleworth, Magnetochemistry, **6**, 61 (2020). https://doi.org/10.3390/magnetochemistry6040061
[77] C. Leroux, M.C. Cadeville, V. Pierron-Bohnes, G. Inden, and F. Hinz, J. Phys. F: Met. Phys. **18**, 2033 (1988). https://doi.org/10.1088/0305-4608/18/9/021
[78] N.I. Vlasova, G.S. Kandaurova, and N.N. Shchegoleva, J. Magn. Magn. Mater. **222**, 138 (2000). https://doi.org/10.1016/s0304-8853(00)00506-0
[79] M.J. Capitan, S. Lefebvre, Y. Calvayrac, M. Bessiere, and P. Cenedese, J. Appl. Crystallogr. **32**, 1039 (1999). https://doi.org/10.1107/s002188989900998x
[80] R.J. Soulen Jr., J.M. Byers, M.S. Osofsky, B. Nadgorny, T. Ambrose, S.F. Cheng, P.R. Broussard, *et al.*, Science, **282**, 85 (1998). https://doi.org/10.1126/science.282.5386.85
[81] F. Goumrhar, L. Bahmad, O. Mounkachi, and A. Benyoussef, Comput. Condens. Matter, **15**, 15 (2018). https://doi.org/10.1016/j.cocom.2018.03.003
[82] R.J. Lange, S.J. Lee, D.W. Lynch, P.C. Canfield, B.N. Harmon, *et al*., Phys. Rev. B, **58**, 351 (1998). https://doi.org/10.1103/PhysRevB.58.351
[83] I. Galanakis, M. Alouani, and H. Dreyssé, Phys. Rev. B, **62**, 6475 (2000). https://doi.org/10.1103/physrevb.62.6475
[84] M. Born, and K. Huang, *Dynamical Theory of Crystal Lattices*, (Clarendon Press, Oxford, 1956).
[85] W. Voigt, Ann. Phys. **38**, 573 (1889). https://doi.org/10.1002/ange.18890022003
[86] A. Reuss, Z. Angew. Math. Mech. **9**, 49 (1929). https://doi.org/10.1002/zamm.19290090104
[87] R. Hill, Proc. Phys. Soc. Lond. A 65 (1952) 349.
[88] C.H. Jenkins, and S.K. Khanna, *Mechanics of Materials*, (Elsevier, 2005).

[89] S.F. Pugh, Philos. Mag. **45**, 823 (1954). https://doi.org/10.1080/14786440808520496
[90] D.G. Pettifor, Mater. Sci. Technol. **8**, 289 (1992). https://doi.org/10.1007/978-1-4615-3382-5_17
[91] X.-Q. Chen, H. Niu, D. Li, and Y. Li, Intermetallics, **19**, 1275 (2011). https://doi.org/10.1016/j.intermet.2011.03.026
[92] O.L. Anderson, J. Phys. Chem. Solids, **24**, 909 (1963). https://doi.org/10.1016/0022-3697(63)90067-2
[93] Y. Pan, and M. Wen, Vacuum, **156**, 419 (2018). https://doi.org/10.1016/j.vacuum.2018.08.010
[94] Nianyi, W. Shangan, Z. Yong, and Z. Xiangyun, J. Alloys Compd. **234**, 130 (1996). https://doi.org/10.1016/0925-8388(95)01963-4
[95] Q. Chen, Z. Huang, Z. Zhao, and C. Hu, Comput. Mater. Sci. **67**, 196 (2013). https://doi.org/10.1016/j.commatsci.2012.08.010
[96] G. Inden, in: *Proc. Int. Conf. on Solid-Solid Phase Transformations, TMS-AIME*, (Warrendale, PA, 1983), pp. 175.
[97] J.M. Sanchez, J.L. Moran-Lopez, C. Leroux, and M.C. Cadeville, J. Phys. : Condens. Matter, **1**, 491 (1989). https://doi.org/10.1088/0953-8984/1/2/019
[98] S.I. Ranganathan, and M. Ostoja-Starzewski, Phys. Rev. Lett. **101**, 055504 (2008). https://doi.org/10.1103/physrevlett.101.055504
[99] X. Luan, Q. Zhang, H. Bao, J. Zhou, B. Zhang, G. Wu, and J. Li, Crystals, **8**, 307 (2018). https://doi.org/10.3390/cryst8080307
[100] X. Li, X. Chen, L. Han, C. Ruan, P. Lu, and P. Guan, J. Mater. Res. **31**, 2956 (2016). https://doi.org/10.1557/jmr.2016.307
[101] M.A. Blanco, E. Francisco, and V. Luaña, Comput. Phys. Commun. **158**, 57 (2004). https://doi.org/10.1016/j.comphy.2003.12.001
[102] P.L. Dulong, and A.T. Petit, Ann. Chim. Phys. **10**, 395 (1819).

AB-INITIO ДОСЛІДЖЕННЯ ФІЗИЧНИХ ОСОБЛИВОСТЕЙ ІНТЕРМЕТАЛІДІВ Pt-Co

Х. Гримед[1,2], Р. Булехфар[1], Х. Бен Садаллах[1], Ф. Семарі[4], Й. Хеніуї[5], Д. Саяд[3], М. Буджелал[4], Х. Мераджи[6], С. Гемід[6], Д. Сінгх[7], Р. Кената[4,8]

[1]Лабораторія матеріалознавства та енергетичної інженерії (LMGE), Університет від 20 серпня 1955 р., Скікда, Алжир
[2]Лабораторія LRPCSI, Університет від 20 серпня 1955 р., поштова скринька 26, Скікда, 21000, Алжир
[3]Лабораторія електроніки Скікди (LRES), Кафедра електротехніки, Університет від 20 серпня 1955 р., Скікда, 21000, Скікда, Алжир
[4]Лабораторія квантової фізики речовини та математичного моделювання, Університет Маскари, 29000, Маскара, Алжир
[5]Кафедра структурних та облицювальних матеріалів, Відділ паливних технологій, Ядерний дослідницький центр Драрія, П/с А/с 43, Себала, Драрія, Алжир, Алжир
[6]Лабораторія радіаційної фізики, кафедра фізики, факультет природничих наук, Університет Баджі Мохтара, Аннаба, Алжир
[7]Кафедра фізики, Інститут фізичних наук для вивчення та досліджень ім. професора Раджендри Сінгха (Раджу Бхайя), Університет Віра Бахадура Сінгха Пурванчала, Джаунпур-222003, Університетський патріархат, Індія
[8]Алжирська академія наук і технологій, Райс Хаміду Вілла-Ель-Маданія, Алжир 16000, Алжир

У цій статті досліджуються структурні, електронні, механічні, магнітні та термодинамічні властивості інтерметалевих сполук Pt-Co за допомогою методу FP-LAPW (повнопотенціальна лінеаризована доповнена плоска хвиля) в рамках DFT (теорії функціоналу густини), реалізованого в коді Wien2k. Негативні ентальпії утворення та енергії когезії вказують на те, що Pt_3Co ($L1_2$), PtCo ($L1_0$) та $PtCo_3$ ($L1_2$) стабільні у феромагнітній (FM) фазі. Розрахунки постійних кристалічної решітки та модуля об'ємної пружності узгоджуються з існуючими теоретичними та експериментальними значеннями. Отримана електронна зонна структура встановлює металеву природу та магнітний характер усіх трьох досліджуваних сполук. Визначено глибину нагріву на рівні Фермі, коефіцієнт електронної теплоємності γ_{th}, поляризацію P% та магнітний момент. Дослідження пружних та механічних характеристик показує, що вибрані матеріали є стабільними та злегка анізотропними. Матеріали Pt_3Co та $PtCo_3$ є за своєю суттю пластичними, а PtCo є твердішою сполукою. Для кращого розуміння цих матеріалів застосовується квазігармонічна модель Дебая для вивчення їхніх теплових властивостей.

Ключові слова: *DFT; FP-LAPW; інтерметалід; електронні властивості; механічні константи*